Graph-Cut Segmentation of Retinal Layers from OCT Images

Bashir Isa Dodo, Yongmin Li, Khalid Eltayef and Xiaohui Liu
Department Of Computer Science, Brunel University, United Kingdom
Bashir.Dodo@brunel.ac.uk, Yongmin.Li@brunel.ac.uk, Khalid.Eltayef@brunel.ac.uk XiaoHui.Liu@brunel.ac.uk

Keywords: Retinal layer segmentation, Optical Coherence Tomography, Graph-Cut

Abstract: The segmentation of various retinal layers is vital for diagnosing and tracking progress of medication of various ocular diseases. Due to the complexity of retinal structures, the tediousness of manual segmentation and variation from different specialists, many methods have been proposed to aid with this analysis. However image artifacts, in addition to inhomogeneity in pathological structures, remain a challenge, with negative influence on the performance of segmentation algorithms. Previous attempts normally pre-process the images or model the segmentation to handle the obstruction but it still remains an area of active research, especially in relation to the graph based algorithms. In this paper we present an automatic retinal layer segmentation method, which is comprised of fuzzy histogram hyperbolization and graph cut methods to segment 8 boundaries and 7 layers of the retina on 150 OCT B-Sans images, 50 each from the temporal, nasal and centre of foveal region. Our method shows positive results, with additional tolerance and adaptability to contour variance and pathological inconsistency of the retinal structures in all regions.

1 INTRODUCTION

Segmentation is the separation of images into more meaningful information based on similarity or difference, continuity or discontinuity. Segmentation using graph cut methods, depends on assignment of appropriate weight. The paths obtained by the default shortest path algorithms, have no optimal way of handling inconsistencies (such as the irregularity in OCT images), as thus it sometimes obtains the wrong paths, which we call the "wrong short-cuts". To avoid the wrong short-cuts, we reassign the weights to promote the homogeneity between adjacent edges using fuzzy histogram hyperbolization. In other words, the edges with high value get higher weights, while those with low values become lower. The idea behind this is that, the transition between layers of OCT images which are from dark to light or vice versa are improved. This means we can better identify the layers by searching for the changes or transitions between layer boundaries. Additionally, we take into account the transition between the layers is in most cases very smooth, making it quite difficult to segment the layers. Now if we re-emphasize on this changes, such that they become clearer, this aids the algorithm in successful segmentation and avoiding wrong short-cuts.
In this paper we take into account the effect of promoting continuity and discontinuity, in addition to adding hard constraints based on the structure of retina to segment 7 retinal layers including the Nerve Fibre Layer (NFL), the Ganglion Cell to Layer-Inner Plexiform Layer(GCL+IPL), the Inner Nuclear Layer (INL), the Outer Plexiform Layer (OPL), the Outer Nuclear Layer to Inner Segment (ONL+IS), the Outer Segment (OS) and the Retinal Pigment Epithelium (RPE) by detecting eight (8) layer boundaries. The locations of these layers and boundaries in an OCT image are illustrated in Fig.1. This paper is organized as follows. In Section 2, we review background information on the Graph-Cut segmentation method and the previous work in retinal layer segmentation. Section 3 describes the proposed segmentation method. Section 4 presents experimental results on 150 OCT images. Finally conclusions are drawn in Section 5.

2 BACKGROUND

2.1 The Graph-Cut Method

Graph-Cut is an optimization method used in solving many image processing and computer vision problems, as first reported by (Seheult et al., 1989), where the problem is represented as a graph. A graph G is a pair (ν, ε) consisting of a vertex set ν (referred to as nodes in 2D or Vertex 3D nested grid) and an edge

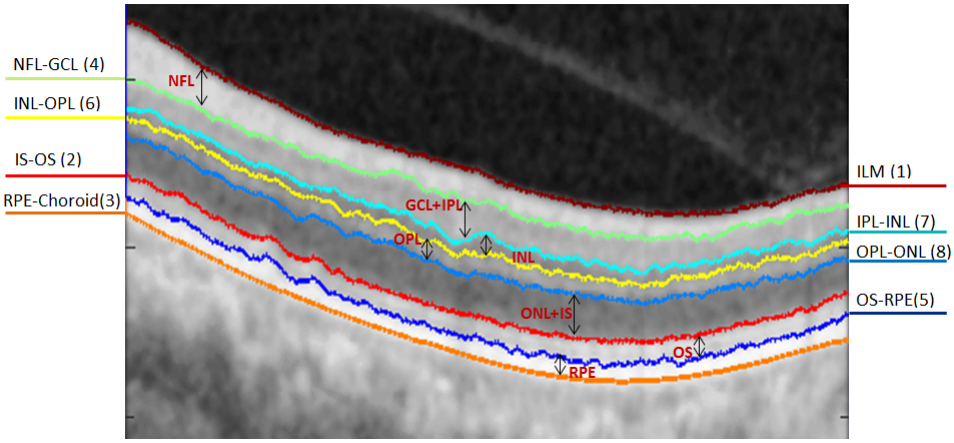

Figure 1: Illustration of the 8 boundaries and 7 retinal layers segmented in the study. The numbers in brackets are the sequential order of the segmentation.

set $\varepsilon \subset \nu$ x ν. There are two main terminal vertices, the source s and the sink t. The edge set comprises of two type of edges: the spatial edges $en = (r,q)$, where $r,q \in \nu\backslash\{s \setminus t\}$, stick to the given grid and link two neighbour grid nodes r and q except s and t; the terminal edges or data edges, i.e. $e_s = (s,r)$ or $e_t = (r,t)$, where $r \in \nu\backslash\{s \setminus t\}$, link the specified terminal s or t to each grid node p respectively. Each edge is assigned a cost $C(e)$, assuming all are non-negative i.e. $C(e) \geq 0$. A cut partitions the image into two disjoint sets of s and t, also termed the s-t cut. it divides the spatial grid nodes of Ω into disjoint groups, whereby one belongs to source and the other belongs to the sink, such that

$$\nu = \nu_s \bigcup \nu_t, \nu_s \bigcap \nu_t = \emptyset \tag{1}$$

We then introduce the concept of max-flow/min-cut(Ford and Fulkerson, 1956). For each cut, the energy is defined as the sum of the costs C(e) of each edge e $\in \varepsilon_{st} \subset \varepsilon$, where its two end points belong to two different partitions. Hence the problem of min-cut is to find two partitions of vertices such that the corresponding cut-energy is minimal,

$$\min_{\varepsilon_{st} \subset \varepsilon} \sum_{e \in \varepsilon_{st}} C(e) \tag{2}$$

while on the other hand the max-flow is used to calculate the maximal flow allowed to pass from the source s to the sink t, and is formulated by

$$\max_{p_s} \sum_{v \in \nu\backslash\{s,t\}} p_s(v) \tag{3}$$

Graph-Cut has been an active area of research since its introduction to image processing, in particular some popular methods utilizing its concept includes (Boykov and Jolly, 2001; Kolmogorov and Zabih, 2004; Yuan et al., 2010).

2.2 SEGMENTATION OF RETINAL LAYERS

The segmentation of retinal layers has been an area of active research and has drawn a large number of researches, since the introduction of Optical Coherence Tomography (OCT) (Huang et al., 1991). Various methods have been proposed, some with focus on number of layers, others on the computational complexity, graph formulation and mostly now optimization approaches. Segmentation of retinal images is challenging and requires automated analysis methods (Baglietto et al., 2017). In this regard a multi-step approach was developed by (Baroni et al., 2007). However the results obtained were highly dependent on the quality of images and the alterations induced by retinal pathologies. A 1-D edge detection algorithm using the Markov Boundary Model (Koozekanani et al., 2001), which was later extended by (Boyer et al., 2006) to obtain the optic nerve head and RNFL. Seven layers were obtained by (Cabrera Fernández et al., 2005) using a peak search interactive boundary detection algorithm based on local coherence information of the retinal structure. The Level Set method was used by (Novosel et al., 2013; Wang et al., 2015b; Wang et al., 2015a; Wang et al., 2017) which were computationally expensive compared to other optimization methods. Graph based methods in (Salazar-Gonzalez et al., 2014; Kaba et al., 2015; Zhang et al., 2015; Haeker et al., 2007; Garvin et al., 2009) have reported successful segmentation results, with varying success rates.Recently, (Dodo et al., 2017) proposed a method using the Fuzzy Histogram Hyperbolization (FHH) to improve the image quality, then embedded the image into the continuous max-flow to simultaneously segment 4 retinal layers.

Moreover, the use of gradient information derived from the retinal structures has in recent years been of interest to OCT segmentation researchers. It was utilised by (Chiu et al., 2010) with the Graph-Cut method, where the retinal structure is employed to limit search space and reduced computational time with dynamic programming. This method was recently extended to 3D volumetric analysis by (Tian et al., 2015) in OCTRIMA 3D with edge map and convolution kernel in addition to hard constraints in calculating weights. They also exploited spatial dependency between adjacent frames to reduce processing time. Edge detection and polynomial fitting was yet another approach proposed to derive boundaries of the retinal layers from gradient information by (Lu et al., 2011), and machine learning by (Lang et al., 2013) with the use of random forest classifier. The utilization of gradient information on OCT images is largely based on the changes that occur at layer boundaries in the vertical direction, thereby attracting segmentation algorithms to exploit this advantage. Our method takes into account the retinal structure and gradient information, but more importantly, the re-assignment of weights in the adjacency matrix, which contributes largely to the success of our graph-cut approach.

3 THE PROPOSED METHOD

In this section we provide the details of our approach to segmenting 8 retinal layer boundaries from OCT B-Scan images.A schematic representation of the overall method is illustrated in Fig. 4

3.1 Pre-Processing

The speckle noise is very common in OCT images, which has negative effects on further processing, for example, the retinal OCT images have low Signal to Noise Ratio (SNR) due to the strong amplitude of speckle noise. Various methods have been used to handle the presence of noise. In this work, we preprocess the images with a Gaussian filter to suppress the speckle noise and enhance the retinal layer boundaries, which is important for the weight calculation in the next stage. This also reduces false positive in the segmentation stage. We show example of a preprocessed image compared to its original in Fig. 2 .

3.2 Weight Calculation

In this stage we obtain the vertical gradient of the image, normalize the gradient image to values in the range of 0 to 1, and then we obtain the inverse of the normalized image gradient as shown in Fig. 3. These two normalized gradient images are then used to obtain two separate undirected adjacency matrices, where Fig. 3(a) contains information of light-dark transitions while 3(b) contains information for transition from dark-light. The adjacency matrices are formulated with the following equation (Chiu et al., 2010):

$$w_{ab} = 2 - g_a - g_b + w_{min} \tag{4}$$

where w_{ab}, g_a, g_b and w_{min} are the weights assigned to the edge connecting any two adjacent nodes a and b, the vertical gradient of the image at node a, the vertical gradient of the image at node b, and the minimum weight added for system stabilization. To improve the continuity and homogeneity in the adjacency matrices they are hyperbolized, firstly by calculating the membership function with the fuzzy sets equation (5) (Tizhoosh et al., 1997) and then transformed with equation (6).

$$w'_{ab} = \frac{w_{ab} - w_{mn}}{w_{mx} - w_{mn}} \tag{5}$$

where w_{mn} and w_{mx} represents the maximum and minimum values of the adjacency matrix respectively, the adjacency matrices are then transformed with the following equation:

$$w''_{ab} = (w'_{ab})^{\beta} \tag{6}$$

where w'_{ab} is the membership value from (5), and β, the fuzzifier is a constant. Considering the number of edges in an adjacency matrix, we use a constant β instead of calculating the fuzziness. The main reason is to reduce computational time and memory usage. The resulting adjacency matrices are such that the weights are reassigned, and the edges with high weights get higher values while those with low values get lower edge weights. Our motive here is that, if continuity or discontinuity is re-emphasized the algorithm will perform better. Where in this case we improve both, the region of the layers get values close to each other, while that of the background gets lower along the way, this is more realistic and applicable in this context (as the shortest path is greedy search approach), because at the boundary of each layer there is a transition from bright to dark or dark to bright, and therefore improving it aids the algorithm in finding correct optimal solutions that are very close to the actual features of interest.

The weight calculation is followed by several sequential steps of segmentation that are discussed in

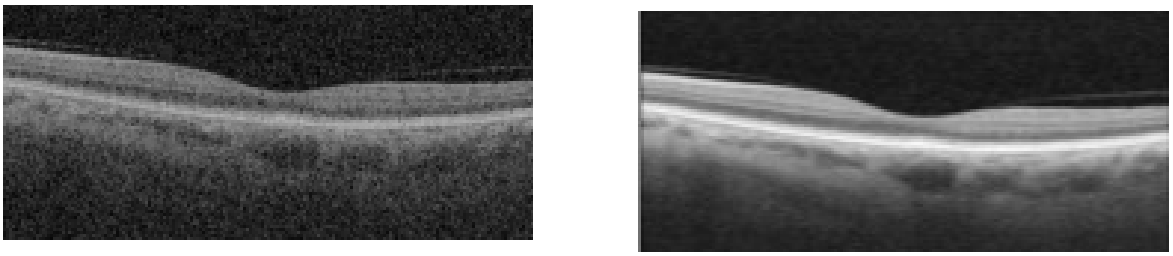

Figure 2: Image pre-processing. (a) Original image corrupted with speckle noise, and (b) filtered image by Gaussian.

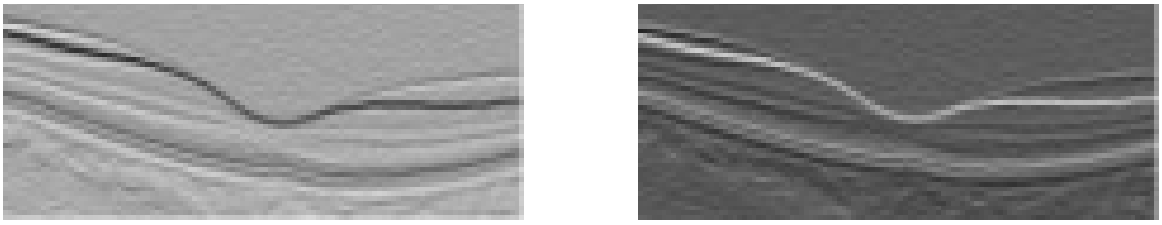

Figure 3: Image gradients used in generating (a) dark-bright adjacency matrix and (b) bright-dark adjacency matrix

the next few subsections. We adopt layer initialization from (Chiu et al., 2010), where two columns are added to either side of the image with minimum weights (w_{min}), to enable the cut move freely in those columns. This is based on the understanding that each layer extends from the first to last column of the image, i.e. dividing the image horizontally at each layer boundary, and that the Graph-Cut method prefers paths with minimum weights. We use Djikstra's algorithm (Dijkstra, 1959) in finding the minimum weighted path in the adjacency matrix (other optimization methods utilizing sparse adjacency matrices might be used in finding the minimum path). Graph-Cut methods are optimal at finding one boundary at a time, and therefore to segment multiple regions in most cases, requires an iterative search in limited space. Limiting the region of search is a complex task, it requires prior knowledge and is dependent on the structure of the features or regions of interest. Some additional information on automatic layer initialization and region limitation are discussed in (Chiu et al., 2010) and (Kaba et al., 2015).

3.3 ILM and IS-OS segmentation

It is commonly accepted that the NFL, IS-OS and RPE exhibits high reflectivity in an OCT image (Chiu et al., 2010; Lu et al., 2011; Tian et al., 2015). Taking into account this reflectivity and the dark-bright adjacency matrix we segment the ILM and IS-OS boundaries using Dijkstras algorithm (Dijkstra, 1959). The ILM (vitreous-NFL) boundary is segmented by searching for the highest change from dark to light, this is because there is a sharp change in the transition, additionally it is amidst extraneous features, above it is the background region in addition to no interruption of the blood vessels, as can be seen in the gradient image. All of the above reasons make it easier to segment the ILM than other layers. We then limit the region below ILM and search for the next highest change from dark-bright in order to segment the IS-OS boundary. In most cases the ILM is segmented, but to account for uncertainties, i.e to differentiate or confirm which layer was segmented, we use the mean value of the vertical axis of the paths to determine the layer segmented, as the ILM is above the IS-OS (similar to (Chiu et al., 2010).

3.4 RPE and NFL-GCL segmentation

As mentioned in the previous subsection, RPE is one of the most reflective layers. Using the bright-dark adjacency matrix, the RPE-Choroid boundary exhibits the highest bright-dark layer transition as can be seen in Fig.3(a). Additionally based on experimental results, it is better to search for the transition from bright to dark for the RPE, due to the interference of blood vessels and the disruption of hyper-reflective pixels in the choroid region. Therefore searching for the bright-dark transition is ideal for the RPE most especially to adapt to noisy images. To segment the NFL-GCL boundary,we limit the search space between ILM to IS-OS, and utilize the bright-dark adjacency matrix to find the minimum weighted path. The resulting path is the NFL-GCL boundary, as it is one of the most hyper-reflective layers. Addition-

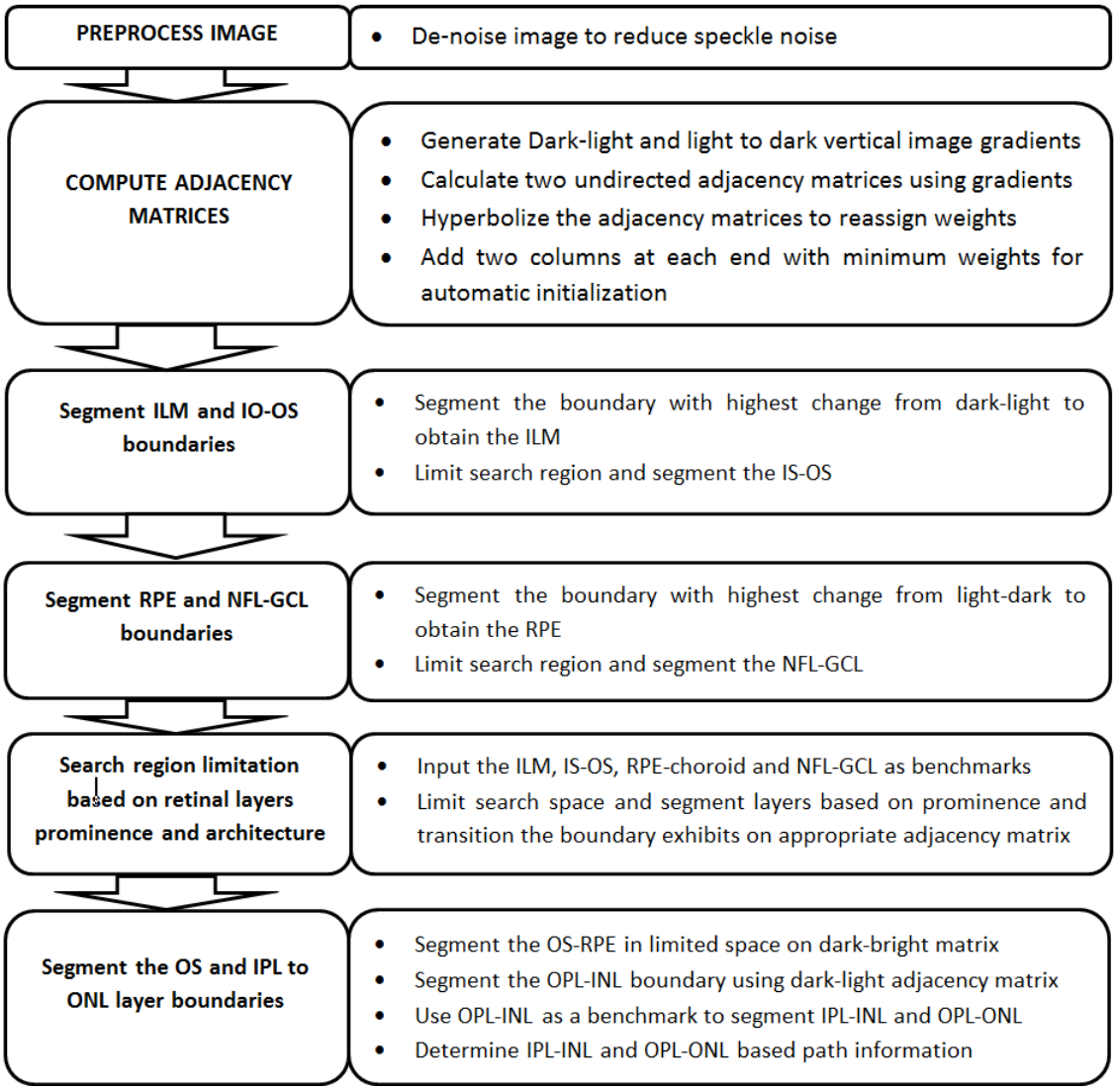

Figure 4: Main steps of segmentation algorithm schematic representation

ally if we limit our search space to regions below the ILM and above the RPE, the resulting bright-dark and dark-bright minimum paths are the NFL-GCL and IS-OS respectively (i.e the NFL-GCL and IS-OS boundaries exhibits the second highest bright-dark and dark-bright transition respectively in an OCT image).

3.5 OS and IPL to ONL Segmentation

To segment the OS-RPE and three other boundaries (IPL-INL, INL-OPL, and OPL-ONL) from IPL to ONL, we use the prior segmented layers as benchmarks for search space limitation. We obtain the OS-RPE region by searching for the dark-bright shortest path between IS-OS and the RPE-Choroid. For the remaining boundaries, first we segment the INL-OPL, because it exhibits a different transition among the three. This is done by searching for the shortest path between NFL-GCL and IS-OS on the dark-bright adjacency matrix. Consequently the IPL-INL and OPL-ONL boundaries are obtained by limiting the region of path search between INL-OPL and NFL-GCL, and INL-OPL and IS-OS regions respectively, on the bright-dark adjacency matrix.

4 EXPERIMENTAL RESULTS

We evaluated the performance of the proposed method on a set of 150 B-scan OCT images centred on the macular region. This data set was collected in Tongren Hospital with a standard imaging protocol for retinal diseases such as glaucoma. The resolution of the B-scan images are 512 pixels in depth and 992 pixels across section with 16 bits per pixel. We manually labelled all the retinal layers in the dataset under the supervision of clinical experts. This serves as the ground truth in our experiments. Prior to segmenting the images, 15% percent of the image height was cropped from the top to remove regions with low signal and no features of interest. We segment seven retinal layers automatically using MATLAB 2016a software. The average computation time was 4.25 seconds per image on a PC with Intel i5-4590 CPU, clock of 3.3GHz, and 8GB RAM memory.

The method obtains the boundaries in the order from ILM(Vitreous-NFL), IS-OS, RPE-Choroid, NFL-GCL, OS-RPE, INL-OPL, IPL-INL to OPL-ONL respectively. The locations of these boundaries and the sequential order of the segmentation is shown in Fig. 1. Sample results of the 8 retinal layer boundaries and the underlying 7 layers are shown in Fig. 5. To evaluate the proposed method we calculate the Root Mean Squared Error (RMSE), and Mean Absolute Deviation (MAD) by (7). Table 1 shows the mean and standard deviation of both MAD and RMSE, for the seven layers targeted in this study.

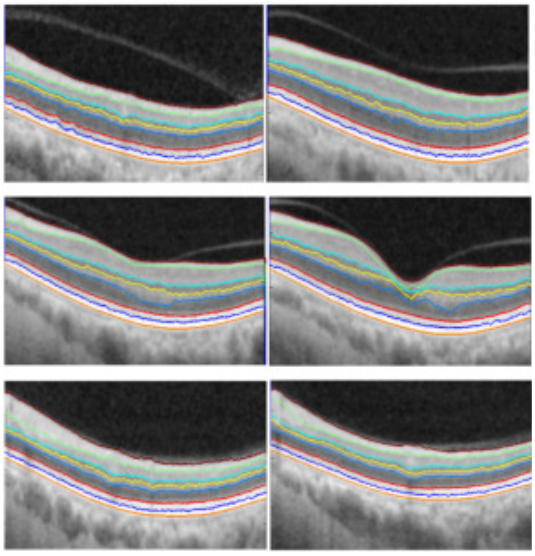

Figure 5: Segmentation results of 8 boundaries and 7 layers. Boundaries from top to bottom, the segmented boundaries are ILM, NFL-GCL, IPL-INL,INL-OPL, OPL-ONL, IS-OS, OS-RPE and RPE-Choroid

$$
\begin{aligned}
&MAD(GT,SEG) = \\
&0.5 * \left(\frac{1}{n}\sum_{i=1}^{n} d(pt_i, SEG) + \frac{1}{m}\sum_{i=1}^{m} d(ps_i, GT) \right) \\
&RMSE = \sqrt{\frac{1}{n}\sum_{i=1}^{n} (SEG_i - GT_i)^2} \\
&Dice \qquad\qquad = \frac{2 \mid GT_i \cap SEG_i \mid}{\mid GT_i \mid + \mid SEG_i \mid}
\end{aligned}
\tag{7}
$$

where SEG_i is the pixel labelled as retinal Layer by the proposed segmentation method and GT_i is the true retinal layers pixel in the manually annotated image (ground truth) image. pt_i and ps_i represent the coordinates of the images, while $d(pt_i, SEG)$ is the distance of pt_i to the closest pixel on SEG with the same segmentation label, and $d(ps_i, GT)$ is the distance of ps_i to the closest pixel on GT with the same segmentation label. n and m are the number of points on SEG and GT respectively. For all layers our method has performed well. Especially considering the low value of NFL for both MAD and RMSE. The high value in ONL+IS is due to the presence of high noise and lower reflectivity of the boundaries within the region, however, this is still considerably low. Furthermore, We evaluated the retinal nerve fibre layer thickness (RNFLT) (the area between ILM and NFL-GCL) with additional criteria, due to its high importance in

Table 1: Performance evaluation with mean and standard deviation of RMSE and MAD for 7 retinal boundaries. 150 SD-OCT B-Scan images (Units in pixels)

RetinalLayer	*MeanMAD*	*MeanRMSE*	*STDMAD*	*STDRMSE*
NFL	0.2689	0.0168	0.0189	0.0121
GCL+IPL	0.5938	0.0432	0.0592	0.0382
INL	0.6519	0.0387	0.0792	0.0612
OPL	0.5101	0.0446	0.0410	0.0335
ONL+IS	0.6896	0.0597	0.0865	0.0329
OS	0.4617	0.0341	0.0360	0.0150
RPE	0.4617	0.0341	0.0360	0.0150

Table 2: Mean accuracy, sensitivity, error rate, Dice and Root Mean Squared Error (RMSE) of the Retinal Nerve Fibre Layer Thickness (RNFLT) and standard deviation (STD).

	Measure	*STD*
Mean Accuracy	0.9816	0.0375
Mean Sensitivity	0.9687	0.0473
Mean Error Rate	0.0669	0.0768
Mean Dice	0.9746	0.0559

the diagnosis of ocular diseases, including glaucoma. This is evaluated with four criteria, namely, accuracy, sensitivity(true positive rate(TPR)), error rate(FPR) and the Dice index(coefficient). These measurements are computed with the following equations while the Dice is computed from (8):

$$\begin{aligned} Accuracy &= \frac{TP+TN}{(TP+FP+FN+TN)} \\ Sensitivity(TPR) &= \frac{TP}{(TP+FN)} \\ ErrorRate(FPR) &= \frac{FP}{(FP+TN)} \end{aligned} \tag{8}$$

where TP, TN, FP and FN refers to true positive, true negative, false positive and false negative respectively. TP represents the number of pixels which are part of the region that are labeled correctly by both the method and the ground truth. TN represents the number of pixels which are part of the background region and labeled correctly by both the method and the ground truth. FP represents the number of pixels labeled as a part of the region by the method but labeled as a part of the background by the ground truth. Finally, FN represents the number of pixels labeled as a part of the background by the system but labeled as a part of the region in ground truth. The results of applying the above criteria on the RNFLT are shown in Table 2.

5 CONCLUSIONS

We have presented an automatic segmentation method for retinal OCT images that is capable of segmenting 7 retinal layers with 8 boundaries. The core of the method is a Graph-Cut segmentation using Dijkstra's algorithm (Dijkstra, 1959). More importantly, the adjacency matrices from vertical gradients and a sequential process of segmentation, as two key elements of the study, are integrated into the Graph-Cut framework. We have applied the proposed method to a dataset of 150 OCT B-scan images, with successful segmentation results. Further quantitative evaluation indicates that the segmentation measurement is very close to the ground-truth.

The main contributions of this work are as follows:

1. We have presented a method to automatically identify 7 retinal layers across 8 layer boundaries, so far one of the most comprehensive studies in this area;
2. The adjacency matrices are effectively integrated into the Graph-Cut framework with better weight calculation;
3. Based on the unique characteristics of reflectivity of different retinal layers and their changes across layers, a sequential process of segmentation has been developed.

REFERENCES

Baglietto, S., Kepiro, I. E., Hilgen, G., Sernagor, E., Murino, V., and Sona, D. (2017). Segmentation of retinal ganglion cells from fluorescent microscopy imaging. In *Proceedings of the 10th International Joint Conference on Biomedical Engineering Systems and Technologies (BIOSTEC 2017)*, pages 17–23.

Baroni, M., Fortunato, P., and La Torre, A. (2007). Towards quantitative analysis of retinal features in optical coherence tomography. *Medical engineering & physics*, 29(4):432–441.

Boyer, K. L., Herzog, A., and Roberts, C. (2006). Automatic recovery of the optic nervehead geometry in optical coherence tomography. *IEEE Transactions on Medical Imaging*, 25(5):553–570.

Boykov, Y. and Jolly, M.-P. (2001). Interactive Graph Cuts for Optimal Boundary & Region Segmentation of Objects in N-D Images. *Proceedings Eighth IEEE International Conference on Computer Vision. ICCV 2001*, 1(July):105–112.

Cabrera Fernández, D., Salinas, H. M., and Puliafito, C. A. (2005). Automated detection of retinal layer structures on optical coherence tomography images. *Optics Express*, 13(25):10200.

Chiu, S. J., Li, X. T., Nicholas, P., Toth, C. a., Izatt, J. a., and Farsiu, S. (2010). Automatic segmentation of seven retinal layers in SDOCT images congruent with expert manual segmentation. *Optics express*, 18(18):19413–19428.

Dijkstra, E. W. (1959). A note on two problems in connexion with graphs. *Numerische mathematik*, 1(1):269–271.

Dodo, B., Li, Y., and Liu, X. (2017). Retinal oct image segmentation using fuzzy histogram hyperbolization and continuous max-flow. In *IEEE International Symposium on Computer-Based Medical Systems*.

Ford, L. R. and Fulkerson, D. R. (1956). Maximal flow through a network. *Journal canadien de mathématiques*, 8:399–404.

Garvin, M. K., Abràmoff, M. D., Wu, X., Russell, S. R., Burns, T. L., and Sonka, M. (2009). Automated 3-D intraretinal layer segmentation of macular spectral-domain optical coherence tomography images. *IEEE transactions on medical imaging*, 28(9):1436–1447.

Haeker, M., Wu, X., Abràmoff, M., Kardon, R., and Sonka, M. (2007). Incorporation of regional information in optimal 3-D graph search with application for intraretinal layer segmentation of optical coherence tomography images. *Information processing in medical imaging : proceedings of the ... conference*, 20:607–618.

Huang, D., Swanson, E. A., Lin, C. P., Schuman, J. S., Stinson, W. G., Chang, W., Hee, M. R., Flotte, T., Gregory, K., and Puliafito, C. A. (1991). Optical coherence tomography. *Science (New York, N.Y.)*, 254(5035):1178–81.

Kaba, D., Wang, Y., Wang, C., Liu, X., Zhu, H., Salazar-Gonzalez, a. G., and Li, Y. (2015). Retina layer segmentation using kernel graph cuts and continuous max-flow. *Optics express*, 23(6):7366–84.

Kolmogorov, V. and Zabih, R. (2004). What Energy Functions Can Be Minimized via Graph Cuts? *IEEE Transactions on Pattern Analysis and Machine Intelligence*, 26(2):147–159.

Koozekanani, D., Boyer, K., and Roberts, C. (2001). Retinal thickness measurements from optical coherence tomography using a Markov boundary model. *IEEE Transactions on Medical Imaging*, 20(9):900–916.

Lang, A., Carass, A., Hauser, M., Sotirchos, E. S., Calabresi, P. a., Ying, H. S., and Prince, J. L. (2013). Retinal layer segmentation of macular OCT images using boundary classification. *Biomedical optics express*, 4(7):1133–52.

Lu, S., Yim-liu, C., Lim, J. H., Leung, C. K.-s., and Wong, T. Y. (2011). Automated layer segmentation of optical coherence tomography images. *Proceedings - 2011 4th International Conference on Biomedical Engineering and Informatics, BMEI 2011*, 1(10):142–146.

Novosel, J., Vermeer, K. A., Thepass, G., Lemij, H. G., and Vliet, L. J. V. (2013). Loosely Coupled Level Sets For Retinal Layer Segmentation In Optical Coherence Tomography. *IEEE 10th International Symposium on Biomedical Imaging*, pages 998–1001.

Salazar-Gonzalez, A., Kaba, D., Li, Y., and Liu, X. (2014). Segmentation of the blood vessels and optic disk in retinal images. *IEEE journal of biomedical and health informatics*, 18(6):1874–1886.

Seheult, A., Greig, D., and Porteous;, B. (1989). Exact Maximum A Posteriori Estimation For Binary Images. *Journal of the Royal Statistical Society*, Vol. 51(No. 2):271 –279.

Tian, J., Varga, B., Somfai, G. M., Lee, W. H., Smiddy, W. E., and DeBuc, D. C. (2015). Real-time automatic segmentation of optical coherence tomography volume data of the macular region. *PLoS ONE*, 10(8):1–20.

Tizhoosh, H. R., Krell, G., and Michaelis, B. (1997). Locally Adaptive Fuzzy Image Enhancement. In *International Conference on Computational Intelligence*, pages 272–276. Springer.

Wang, C., Kaba, D., and Li., Y. (2015a). Level set segmentation of optic discs from retinal images. *Journal of Medical Systems*, 4(3):213–220.

Wang, C., Wang, Y., Kaba, D., Wang, Z., Liu, X., and Li, Y. (2015b). Automated Layer Segmentation of 3D Macular Images Using Hybrid Methods. *Image and Graphics*, 9217:614–628.

Wang, C., Wang, Y., and Li, Y. (2017). Automatic choroidal layer segmentation using markov random field and level set method. *IEEE journal of biomedical and health informatics*.

Yuan, J., Bae, E., Tai, X.-C., and Boykov, Y. (2010). A study on continuous max- flow and min-cut approaches. *2010 IEEE Conference*, 7:2217–2224.

Zhang, T., Song, Z., Wang, X., Zheng, H., Jia, F., Wu, J., Li, G., and Hu, Q. (2015). Fast retinal layer segmenta-

tion of spectral domain optical coherence tomography images. *Journal of Biomedical Optics*, 20(9):096014.